Chapter 2
Li_2MnSiO_4 Nanostructured Cathodes for Rechargeable Lithium-Ion Batteries

Rosalind June Gummow

2.1 Introduction

Rechargeable lithium-ion battery technology dominates the portable electronics market following the rapid growth in demand since the introduction of the first, commercial lithium-ion battery by Sony in 1990 [1]. Motivated by concerns for global warming and environmental degradation, researchers have focused on extending the use of rechargeable lithium-ion batteries to large-scale applications. Lithium-ion batteries are attractive candidates for these applications due to their high energy density, high efficiency, and long cycle life. These applications include use as power supplies for low emission hybrid and plug-in electric vehicles and as standby storage to mitigate the unavoidable intermittency of renewable energy technologies like solar and wind power [2, 3]. These extended, large-scale applications place increasingly stringent demands on battery performance and demand the development and optimization of new battery chemistries to meet the challenges for commercial acceptance [3, 4]. In large-scale applications, factors such as safety, toxicity, cost, and abundance of raw materials become highly significant. In addition, high charge and discharge rate requirements mean that nanostructured materials are essential to meet performance targets.

The original, commercial secondary lithium-ion batteries were based on a lithium transition metal oxide cathode (e.g., $LiCoO_2$) and a carbon anode [1]. These two electrodes are insertion materials capable of accommodating lithium ions within their lattice, with very little change to the overall structure. During the charge cycle, lithium ions are extracted from the cathode and at the same time the

R.J. Gummow (✉)
College of Science, Technology and Engineering, James Cook University, James Cook Drive, Douglas, Townsville, QLD 4811, Australia
e-mail: rosalind.gummow@jcu.edu.au

K.I. Ozoemena, S. Chen (eds.), *Nanomaterials in Advanced Batteries and Supercapacitors*, Nanostructure Science and Technology,
DOI 10.1007/978-3-319-26082-2_2

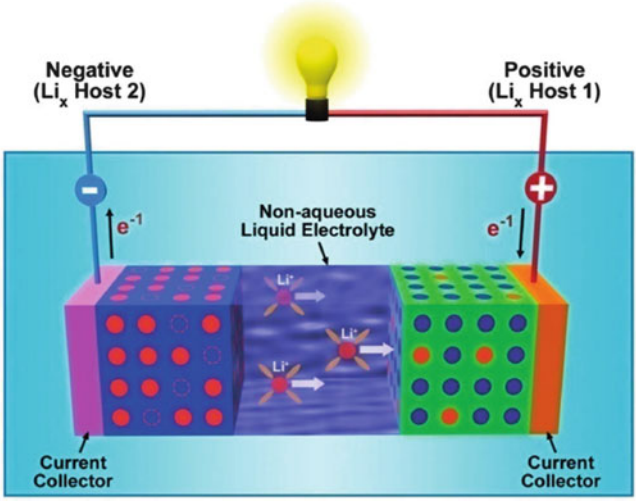

Fig. 2.1 Schematic of a traditional Li-ion battery cell in which, during discharge, Li ions migrate through the electrolyte and electrons flow through the external circuit, both moving from the anode (negative) to the cathode (positive) (Reprinted with permission from Yang Z, Zhang J, Kintner-Meyer MCW, et al. (2011) Chemical Reviews 111:3577–3613. Copyright 2011, American Chemical Society)

transition metal is oxidized. The lithium ions are transported by the electrolyte to the anode where they combine with electrons from the external circuit to form lithium atoms within the carbon matrix. During discharge this process is reversed; lithium atoms at the anode are ionized and lithium ions move through the electrolyte to the anode while electrons move through the external circuit. At the cathode, the lithium ions move into the crystal lattice and the transition metal cations are simultaneously reduced by electrons from the external circuit to maintain charge neutrality. The movement of the lithium ions from anode to cathode and back is the basis of operation of the cells and the origin of the term lithium-ion battery. A schematic diagram of a lithium-ion cell is shown in Fig. 2.1.

Over the years, modifications to the cell chemistry have included changes to the anode, cathode, and electrolyte compositions. The driving force for these innovations has been to increase the electrochemical cell capacity, improve safety and reliability, reduce cost, and increase the reversibility of lithium-ion insertion and extraction with repeated cycling. The performance of electrochemical cells is determined by the crystallographic structure, chemical composition, morphology, and microstructure of electrode materials. In addition, for high rate applications, the optimal nanostructure and architecture of electrodes are essential to provide rapid charge transfer across the electrode/electrolyte interface and fast transfer of lithium ions and electrons within the active material [5]. Significant advances have been made in improving the capacity of anode materials for lithium-ion batteries [6, 7], but finding suitable high-capacity cathode materials to match the anode performance remains a challenge.

Initially, the selection of suitable cathodes was confined to those materials that had a high intrinsic electronic conductivity, for example, the lithium transition metal oxides. Safety concerns and the desire to move away from relatively scarce, toxic, and expensive transition metals, like cobalt, prompted a broadening of the search to include polyanionic compounds like the lithium transition metal phosphates and silicates [8]. The phosphates and silicates were attractive as the strong covalent bonds in the polyanionic units reduce the likelihood of oxygen evolution in the charged state, compared to the oxides [9]. Oxygen evolution poses a hazard when cells are overcharged resulting in undesirable thermal runaway. Polyanionic compounds also offered the possibility of using nontoxic, abundant metals like Fe and Mn to replace the Co and Ni commonly used in lithium transition metal oxide cathodes. Along with their promise of improved safety, however, comes the disadvantage of their low intrinsic electronic conductivity. These cathode materials, when produced as micron-sized particles, show high polarization when charged at high current rates, resulting in very low capacities. It is believed that this polarization is due to both the poor electronic conductivity of the materials resulting in poor charge transfer and the low lithium-ion diffusion rates within the materials. These limitations have driven researchers to explore nanostructuring cathode materials both to increase the surface area to maximize charge transfer and to reduce the diffusion length to minimize the effect of the low lithium diffusion rates [10].

Lithium iron phosphate ($LiFePO_4$), first proposed by Padhi and Goodenough [9] in the 1990s, is the most commercially successful polyanionic cathode to date. $LiFePO_4$ has excellent rechargeability and consists of abundant, nontoxic materials and has proved very attractive for a range of commercial applications. $LiFePO_4$ discharges at ~3.4 V vs. a Li/Li^+ anode with a capacity of 170 $mAhg^{-1}$ (95 % of theoretical capacity). Nanoparticles of $LiFePO_4$ coated with a layer of conductive carbon perform well even at high current rates [11, 12].

The success of $LiFePO_4$ prompted renewed interest in other polyanionic compounds as lithium-ion battery cathodes [13]. In particular, the lithium transition metal orthosilicates Li_2MSiO_4, where M = Mn, Fe, or Ni have attracted the attention of lithium ion battery researchers [14]. In this chapter the potential of Li_2MnSiO_4 as a secondary lithium-ion battery cathode is explored with particular emphasis on the effect of nanostructuring on electrochemical performance. In this chapter, we will first discuss the challenges associated with the use of Li_2MnSiO_4 cathodes, secondly we will consider the advantages of nanostructuring, and thirdly we will review the published data on nanostructured Li_2MnSiO_4 cathodes.

2.2 The Attraction of Li_2MnSiO_4 as a Lithium-Ion Battery Cathode

Among the lithium transition metal orthosilicates Li_2MSiO_4 (where M = Mn, Co, or Ni), Li_2MnSiO_4 offers the greatest potential as a high-voltage, high-energy-density cathode material. Firstly, it is composed of safe, nontoxic, and abundant

elements, offering the possibility for the formation of low-cost cathodes. Secondly, if both lithium ions could be extracted reversibly from Li_2MnSiO_4, the theoretical capacity would be a very attractive 330 $mAhg^{-1}$ (roughly double the capacity of $LiFePO_4$ electrodes), with the cathode operating with both the $Mn^{2+/3+}$ and $Mn^{3+/4+}$ electrochemical couples [15, 16]. Of the three Li_2MSiO_4 cathodes, Li_2FeSiO_4 shows the most stable capacity with cycling but at a relatively low average voltage of ~2.5 V which lowers the energy density of the cathode. Recent studies have indicated that more than one Li ion can be reversibly extracted from Li_2FeSiO_4 although this remains controversial and further studies are needed to confirm this conclusively [13, 17, 18]. Systematic studies of Li_2CoSiO_4 by Bruce et al. [19] showed low capacities and poor reversibility with cycling, and this has been confirmed by other investigators [20]. Li_2MnSiO_4 is the most likely of the three compounds to exhibit reversible extraction of more than one lithium ion per formula unit as the Mn^{4+} state is more stable than Fe^{4+} or Co^{4+} and is predicted to be accessible within the voltage stability range of common electrolytes [14].

2.3 Challenges of Lithium Manganese Orthosilicate (Li_2MnSiO_4) Cathodes

2.3.1 Multiple Structural Forms

All the lithium transition metal silicates, including Li_2MnSiO_4, can exist in a wide variety of structural forms. There are at least four known forms of Li_2MnSiO_4 at ambient pressure [15, 21–23]. In all cases the Li, Mn, and Si cations are in tetrahedral coordination in a distorted hexagonally close-packed oxygen array, but the arrangement of the tetrahedra differs in each case (Fig. 2.2) [24].

In practice, the multitude of structural forms makes the synthesis of well-defined, single-phase products challenging. The most widely studied forms are the orthorhombic polymorphs ($Pmn2_1$ and $Pmnb$) which differ only slightly in thermodynamic stability [25]. The monoclinic $P2_1/n$ polymorph is a high temperature form typically prepared at 900 °C, although it can be synthesized at lower temperatures with the partial substitution of Mn with Mg [22, 26]. The Pn polymorph has only been prepared by ion exchange from the sodium analogue [23]. The analysis of the cathodes is complicated by the fact that the materials frequently contain multiple phases of Li_2MnSiO_4 as well as secondary impurity phases like MnO and Li_2SiO_3. This complexity makes the production of well-defined and reproducible samples difficult, and small changes in the synthesis conditions can result in very different phase compositions with resulting differences in electrochemical performance.

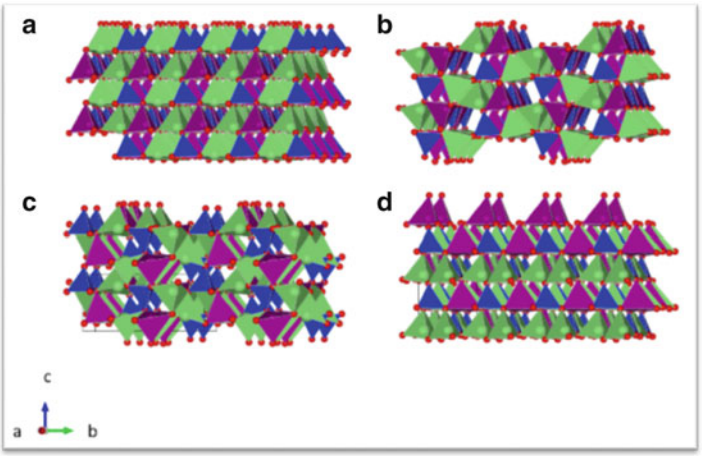

Fig. 2.2 Crystal structures of the four known ambient pressure polymorphs of Li_2MnSiO_4 (**a**) *Pmn*2_1, (**b**) *Pmnb*, (**c**) *P*2_1/*n*, and (**d**) *Pn*. Li tetrahedra are shown in *green*, Mn tetrahedra in *purple*, and Si tetrahedra in *blue*; *red spheres* represent oxygen atoms (Reprinted from Gummow and He [24], copyright (2014), with permission from Elsevier)

2.3.2 Low Lithium-Ion Diffusion Rates

The lithium-ion diffusion pathways in the different structural forms of Li_2MnSiO_4 are distinctly different. The orthorhombic forms *Pmn*2_1 and *Pmnb* (Fig. 2.2a and b) have two-dimensional pathways for lithium-ion diffusion, while the monoclinic forms (*P*2_1/*n* and *Pn*) have lithium positions connected in three dimensions (Fig. 2.2c and d). Calculations have shown that the lithium-ion diffusion pathways in these materials are curved and anisotropic and that all are poor conductors of lithium ions [27, 28]. This finding suggests that lithium diffusion in Li_2MnSiO_4 electrodes may be limiting in high rate applications.

2.3.3 Low Electronic Conductivity

In Li_2MnSiO_4, MnO_4 tetrahedra are surrounded by insulating SiO_4 tetrahedra resulting in very low intrinsic conductivity. The conductivity of Li_2MnSiO_4 at room temperature is of the order of 10^{-16} Scm^{-1} but increases a 100-fold at 60 °C [29, 30]. Unfortunately, this is the case for all structural forms of Li_2MnSiO_4, and this is confirmed by calculations of the band gap for different structural forms [28]. This low conductivity means that the material is effectively electrochemically inactive when particles are micron sized. Without nanostructuring, Li_2MnSiO_4 is completely ineffective as a cathode material but nanostructuring and carbon coating dramatically increase the electrochemical performance and offer hope that the

potential of this material may be realized in practice. For Li_2MnSiO_4, as with other polyanionic materials with low intrinsic electronic and ionic conductivity, nanostructuring is essential to achieve reasonable electrochemical performance.

2.3.4 Volumetric Changes and Amorphization

Density functional theory calculations indicated that the extraction of both lithium ions from Li_2MnSiO_4 should be feasible within the electrolyte stability window of common electrolytes [25]. However, density functional theory simulations by Kokalj et al. [30] also indicated that there is a dramatic volume change associated with extraction of more than 1 Li per formula unit in Li_2MnSiO_4 ($-17\,\%$ for $Li_{0.5}MnSiO_4$ and $-27\,\%$ for $MnSiO_4$). It appears that such large volumetric changes cannot be accommodated within the crystallographic structure and lead to structural collapse and amorphization when lithium is extracted [29, 31].

2.4 Advantages of Nanostructuring Li_2MnSiO_4 Cathodes

2.4.1 Carbon Coating

Carbon is an excellent electronic conductor. When nanoparticles of a poorly conducting electrode material are coated with a layer of carbon, this increases the conductivity of the composite electrode. The carbon coating acts as a distributed current collector and provides a continuous pathway for rapid electronic conduction throughout the nanostructured electrode. In this way, the contact resistance between adjacent particles is dramatically reduced [32]. Thin carbon coatings are also generally permeable to Li ions and therefore do not inhibit the diffusion of lithium into the active material. Reduction of the internal resistance of the composite cathode results in a reduction in polarization at high current densities and therefore in increased high-rate capacities. Excess carbon in composite electrodes decreases the overall energy density of the electrode, and therefore the amount of carbon should be kept to a minimum.

2.4.2 Maximizing the Surface Area

In nanosize particles the surface-to-volume ratio is maximized. This implies that there is a greater area for interaction between the electrolyte and the electrode particles. This results in reduced polarization and greater utilization of the electrode material. However, the increased surface area for interaction can potentially result

in problems with nanostructured cathode materials if they are unstable in contact with the electrolyte, leading to increased degradation of the electrode surface. In this case, carbon coating has the advantage of reducing the interaction between the active material and the electrolyte and effectively stabilizing the interface.

2.4.3 Reducing the Lithium-Ion Diffusion Length

Due to the low lithium-ion diffusion rate in Li_2MnSiO_4 discussed in Sect. 3.2, nanostructuring is important to reduce the lithium-ion diffusion length, i.e., the length that Li ions need to diffuse from the surface of the individual particles into the bulk. This becomes increasingly critical at high current rates. Nanostructuring reduces polarization at high current rates and enables higher capacities to be obtained from cathodes before the voltage cutoff is reached.

2.5 Synthesis and Electrochemistry of Nanostructured Li_2MnSiO_4

2.5.1 Pechini Sol–Gel Synthesis

From the outset, it was recognized that minimizing particle size and incorporating a carbon coating were critical to achieving optimized electrochemical performance in Li_2MnSiO_4 cathodes. Pechini sol–gel synthesis was adopted by Dominko [15] and co-workers in their pioneering work to prepare 70 nm particles of the $Pmn2_1$ form. In their initial report, although there were islands of carbon between particles, there was no discrete carbon coating. The results of electrochemical tests were disappointing, yielding reversible capacities corresponding to only 0.6 Li ions on the first discharge cycle followed by a rapid capacity fade on subsequent cycles [15] (Fig. 2.3a). Refinements to the synthesis technique in later studies reduced the particle size to 20–50 nm (Fig. 2.3b and c), with a uniform distribution of ~5 wt% of carbon, but this failed to improve the room temperature electrochemical cycling performance compared to the earlier studies [16]. Electrochemical cycling experiments at 60 °C showed a plateau near 4 V corresponding to the extraction of 1.5 Li ions but this capacity was not recovered on discharge. It was not clear if this observed charge capacity corresponded to Li extraction or to irreversible side reactions with the electrolyte at high voltage. Even after ball milling to reduce the particle size and improve the distribution of carbon, there was only a slight reduction in polarization. All samples consistently showed a rapid loss of electrochemical capacity with repeated charge–discharge cycling. Even after adopting the same nanostructuring tactics that had proved so successful with $LiFePO_4$, the

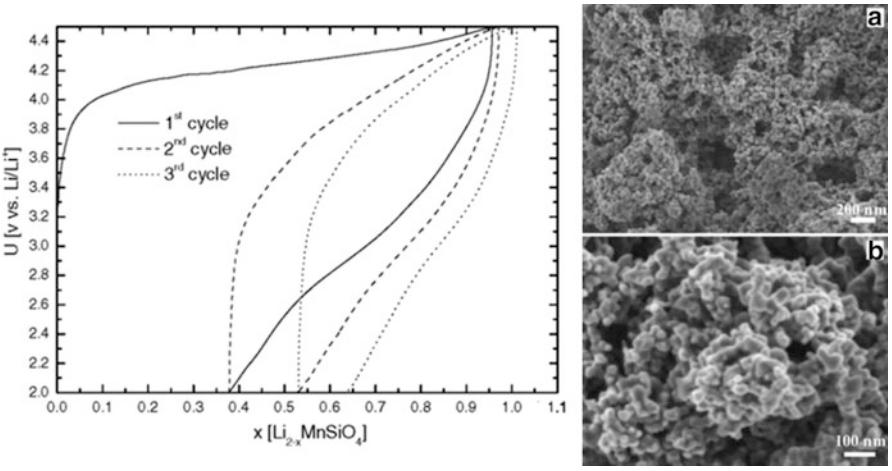

Fig. 2.3 (**a**) Voltage profiles of Li_2MnSiO_4 cycled at room temperature and at a rate of C/30 (Reprinted from Dominko et al. [15], copyright (2006), with permission from Elsevier). SEM micrographs of (**b**) Li_2MnSiO_4 microstructure and (c) Li_2MnSiO_4 particles (Reprinted from Dominko et al. [16], copyright (2007), with permission from Elsevier)

authors failed to achieve a dramatic improvement in the performance of Li_2MnSiO_4 electrodes.

To understand the persistent loss of capacity with cycling, *ex situ* x-ray diffraction studies of partially charged cathodes were conducted. The results revealed a gradual loss of x-ray peak intensity with lithium extraction on charge and no recovery of the peaks when the cell was subsequently discharged (Fig. 2.4). This indicated that the Li_2MnSiO_4 structure underwent irreversible change when lithium was extracted, and these results were confirmed by Li et al. [31] and by further in situ studies by Dominko et al. [29]. The experimentally observed structural collapse (Fig. 2.4) was attributed to the fact that the crystal lattice was unable to accommodate the large volume changes associated with the extraction of more than one lithium ion per formula unit [30].

2.5.2 Alternative Sol–Gel Routes

Refinements to the sol–gel synthesis route were attempted. Deng et al. [33] used a modified citric acid-assisted route with tetraethyl orthosilicate (TEOS) as the silicon source but, although 10.5 wt% carbon was successfully incorporated in the product, the primary particle size was ~200 nm. The electrochemical cycling results for this product were similar to those found in earlier studies. Belharouak et al. [34] also used a modified sol–gel route with $Si(CH_3COO)_4$ as the silicon source but as-prepared samples had primary particles in the 200–300 nm range. As-prepared samples were effectively electrochemically inactive (Fig. 2.5a).

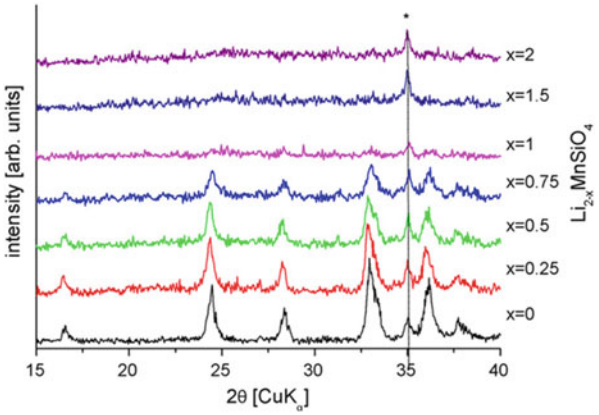

Fig. 2.4 X-ray diffraction patterns of compositions obtained with electrochemical oxidation of Li_2MnSiO_4-based composites. The value of x corresponds to the expected chemical composition of the electrode that is based on the amount of charge passed through the cell. The remaining diffraction peak marked with asterisk denotes MnO impurity (Reprinted from Dominko [29], copyright (2007), with permission from Elsevier)

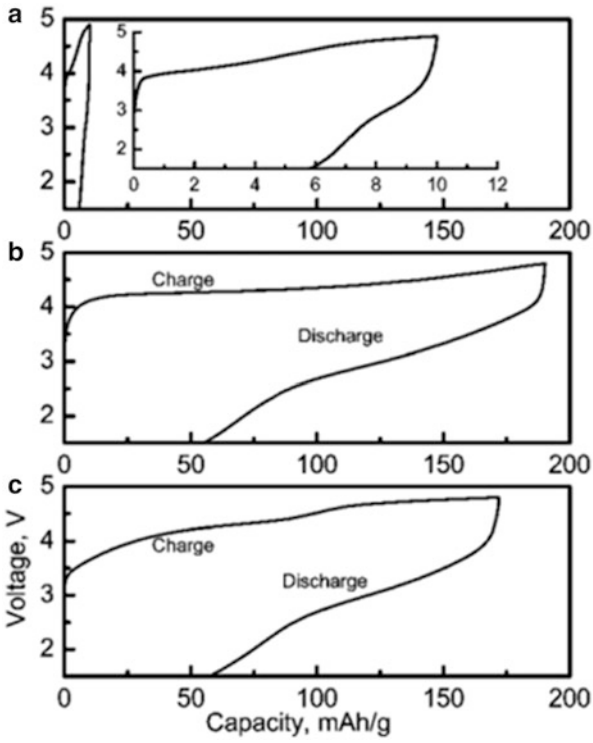

Fig. 2.5 Voltage profiles of (**a**) as-prepared Li_2MnSiO_4, (**b**) carbon-coated Li_2MnSiO_4, and (**c**) high-energy ball-milled Li_2MnSiO_4 (Reprinted with permission from Belharouak et al. [34], copyright (2009) American Chemical Society)

However, dramatic improvement in electrochemical capacity was demonstrated after ball milling to reduce the particle size and coating the particles with a conductive layer of carbon to reduce the charge-transfer resistance and the inter-particle contact resistance (Fig. 2.5b and c). However, even after milling, the particles were agglomerated and the electrochemical capacity remained limited to approximately that equivalent to the reversible extraction, and insertion of one Li ion per formula unit and the capacity retention with cycling was poor.

2.5.3 *Solution Synthesis*

Li et al. [31] adopted a solution synthesis route using Li and Mn acetates with TEOS in a water–ethanol solution refluxed at 80 °C for 24 h. Sucrose was added as a carbon source and the product was calcined at 600 °C in flowing N_2. The final particle size of 20–30 nm was again comparable to that obtained with Pechini synthesis and the structural form of the product was the $Pmn2_1$ polymorph (Fig. 2.6d). The initial discharge capacity obtained with this material in electrochemical cycling tests was 210 $mAhg^{-1}$ at a current rate of 5 mAg^{-1}. This was the first report of a discharge capacity corresponding to insertion of more than 1 Li ion per formula unit (Fig. 2.6c) possibly due to the well-defined carbon coating on the surface of the primary particles shown in the TEM image in Fig. 2.6e. Once again the loss of capacity with repeated cycling was confirmed to be due to a loss of crystallinity with lithium extraction (Fig. 2.6b).

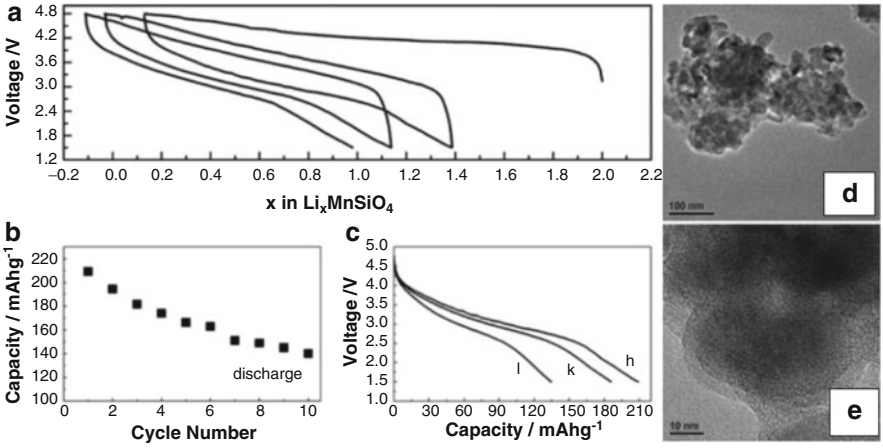

Fig. 2.6 Electrochemical performances of the material: (**a**) voltage vs. composition curves at 5 mAg^{-1}; (**b**) cycling performance between 1.5 and 4.8 V at 5 mAg^{-1}; (**c**) first discharge curves at different current densities: (h) 5 mAg^{-1}; (k) 30 mAg^{-1}; (l) 150 mAg^{-1}.; HRTEM images of Li_2MnSiO_4/C nanocomposite material with different magnifications (**d** and **e**) (Reprinted from Li et al. [31], copyright (2007) with permission from Elsevier)

2.5.4 Polyol Synthesis

Liu et al. [35] adopted a polyol synthesis route for the production of Li_2MnSiO_4. Lithium and manganese acetates and tetraethyl silicate were refluxed in ethylene glycol at 196 °C for 16 h. The product was dried at 150 °C and milled with sucrose to provide a carbon source. After calcination at 600 °C in an inert atmosphere, 30 nm particles of the $Pmn2_1$ polymorph of Li_2MnSiO_4 were formed. The electrochemical cycling performance of this material was comparable to that reported in earlier studies, and the rapid drop in capacity with cycling was again confirmed to be due to a loss of crystallinity when lithium was extracted.

2.5.5 Hydrothermal Synthesis

Sol–gel synthesis techniques and variations thereof failed to result in any dramatic breakthroughs in the performance of Li_2MnSiO_4. Hydrothermal synthesis, in which the precursors are reacted in a sealed autoclave at moderate temperatures but elevated pressures, was introduced as an alternative. This method was initially utilized very successfully to synthesize individual polymorphs of Li_2MnSiO_4 for crystallographic structural investigations [36]. However, no electrochemical evaluation of these materials was performed.

Manthiram et al. [37] used microwave-assisted hydrothermal synthesis to prepare Li_2MnSiO_4 at 30 b and 300 °C. The most significant advantage of this technique is that the synthesis time was reduced to only 25 min resulting in energy saving. After calcination at 650 °C in Ar, the sample consisted of agglomerated 20 nm primary particles with a well-defined layer of carbon on the surface of the particles (Fig. 2.7a and b). Despite high discharge capacities of over 200 $mAhg^{-1}$ on the first two discharge cycles at room temperature (Fig. 2.7c), these materials rapidly lost capacity with repeated charge–discharge cycling. The Jahn–Teller distortion of the manganese cations and dissolution of manganese in the electrolyte

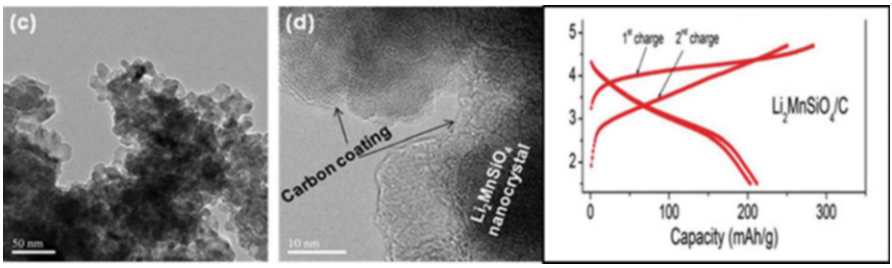

Fig. 2.7 (**a**) TEM and (**b**) HRTEM images of the Li_2MnSiO_4/C nanocomposite. (**c**) Charge–discharge profiles recorded at C/20 rate and room temperature of Li_2MnSiO_4/C (Reprinted with permission Manthiram [37]. Copyright (2010) American Chemical Society)

was given as an explanation for the capacity decline with cycling. The initial discharge capacity at elevated temperature (55 °C) was 250 $mAhg^{-1}$ but the capacity decreased even more rapidly with cycling at this temperature probably due to increased interaction with the electrolyte at the elevated temperature.

2.5.6 *Molten Carbonate Flux Synthesis*

Kojima et al. [38] used a $(Li_{0.435}Na_{0.315}K_{0.25})_2CO_3$ flux with Li_2SiO_3 and either $MnC_2O_4.2H_2O$ or $Mn(OH)_2$ precursors. Reactions were carried out in an atmosphere of CO_2/H_2 100:3 v/v. This method enabled the production of single-phase products of the $Pmn2_1$ form at 500–650 °C, significantly reducing the synthesis temperature compared to conventional sol–gel routes. A key finding was that the choice of manganese precursor dramatically affected the morphology of the final Li_2MnSiO_4 product and this, in turn, resulted in widely different electrochemical performances. The samples with flake-like morphology prepared with $Mn(OH)_2$ precursors (Fig. 2.8b and d) gave higher initial capacities and better capacity retention compared to the more spherical particles prepared with oxalates (Fig. 2.8a and c). However, in both cases, capacity loss with cycling was significant with only 55 % capacity retention after 20 cycles for the better performing samples prepared from $Mn(OH)_2$.

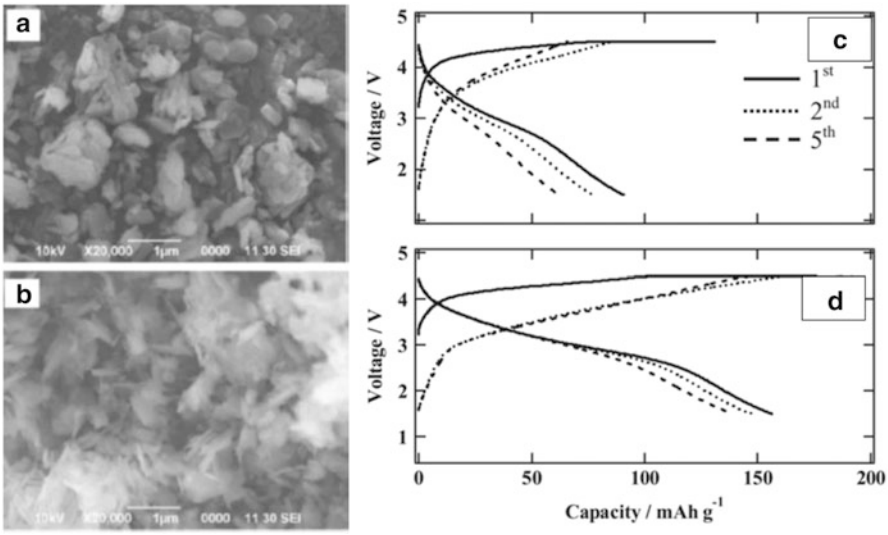

Fig. 2.8 SEM images and charge–discharge curves of the Li_2MnSiO_4 synthesized from $MnC_2O_4.2H_2O$ (LMS-MCO) (**a** and **c**) and manganese hydroxide (LMS-MOH) (**b** and **d**) at 30 °C with a current density of 10 mAg^{-1} in the voltage range of 1.5–4.5 V (Reproduced from Kojima et al. [38], by permission of The Electrochemical Society)

2.5.7 *Supercritical Solvothermal Synthesis*

2.5.7.1 Monodisperse Li_2MnSiO_4 Particles

Supercritical solvothermal synthesis utilizes very high-pressure, moderate temperatures and has the advantage that synthesis times can be reduced to the order of minutes. The requirement of specialized equipment for this type of synthesis would, however, make it expensive and difficult to apply for large-scale manufacture despite the reduced reaction times. This technique was used by Kempaiah et al. [39] to synthesize monodisperse 5–20 nm particles of Li_2MnSiO_4 (Fig. 2.9a–d). The material was found by x-ray diffraction to be a well-defined $Pmn2_1$ polymorph with no obvious impurities. The heat-treated, conductive polymer PEDOT was used for the first time to form a conductive coating on the surface of the particles (Fig. 2.9d). Although excellent capacities were reported for the initial discharge cycle, approaching 300 $mAhg^{-1}$, there was a rapid drop in discharge capacity after the first cycle at room temperature, followed by a gradual decline in subsequent cycles (Fig. 2.10a and c). The capacities reported for cycling at 40 °C were above 250 $mAhg^{-1}$ for the first 20 cycles (Fig. 2.10b and d). It should

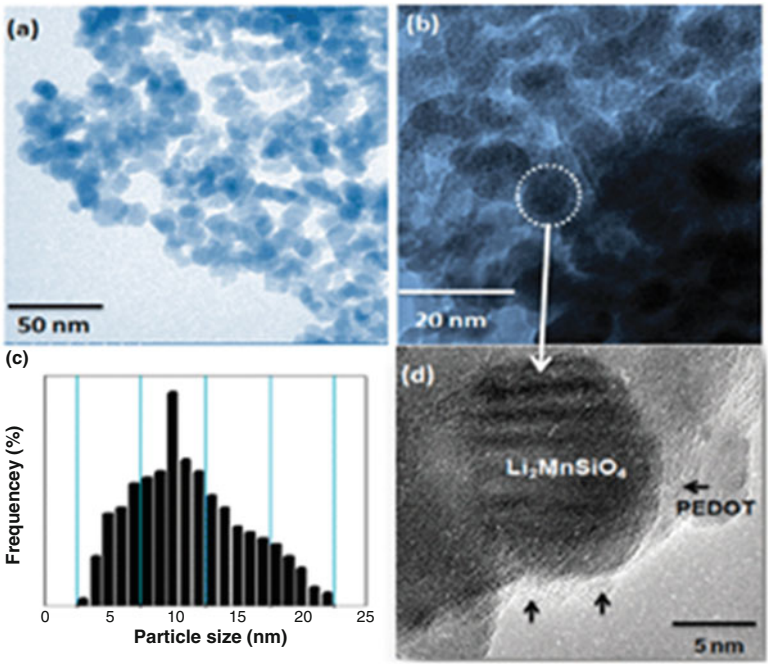

Fig 2.9 (**a**) and (**b**) TEM and HRTEM images of as-synthesized Li_2MnSiO_4 and PEDOT/Li_2MnSiO_4 nanoparticles, (**c**) particle size distribution and (**d**) HRTEM image showing PEDOT-coated Li_2MnSiO_4 nanoparticles (Reproduced from Kempaiah et al. [39] with permission of The Royal Society of Chemistry)

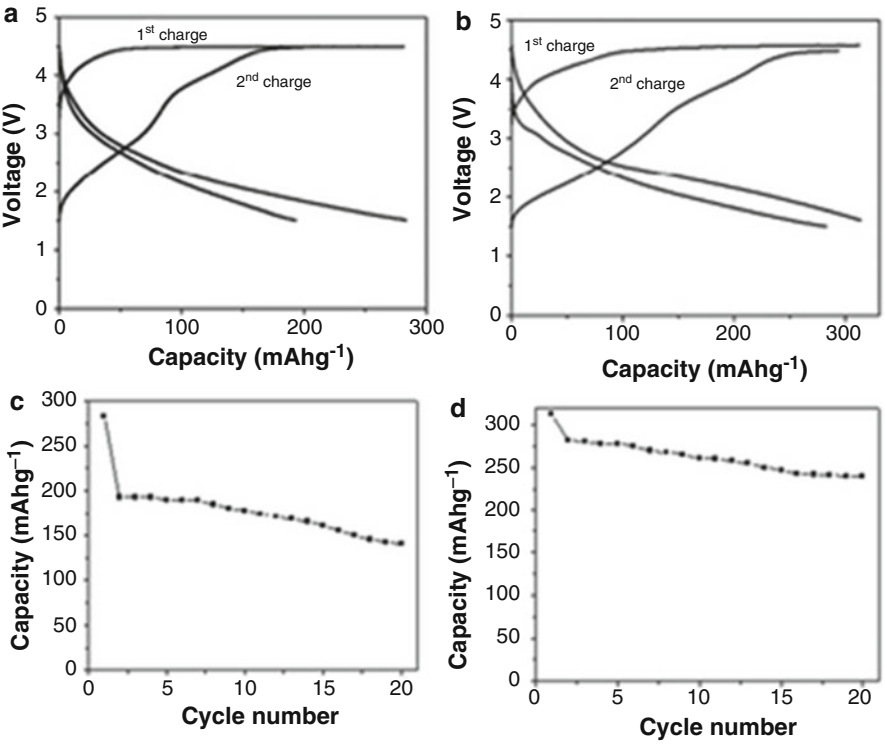

Fig. 2.10 Charge–discharge profiles (**a** and **b**) and cyclic performance (**c** and **d**) of PEDOT/Li_2MnSiO_4 nanoparticles recorded at C/20 in room temperature (**a** and **c**) and at 40 °C (**b** and **d**), respectively (Reproduced from Kempaiah et al. [39] with permission of The Royal Society of Chemistry)

be noted that, although the capacities were high, much of the discharge capacity was recorded at low voltages (below 2.5 V) with only 180 $mAhg^{-1}$ above 2.5 V for the first discharge cycle at 40 °C (Fig. 2.10b); this would reduce the overall energy density of the cathode.

2.5.7.2 Nanosheet Morphology

The success and wide-ranging applications for graphene have prompted great interest in nanosheet morphology [40] The formation of nanosheets only a few nanometers in thickness and with lateral dimensions in the micron range has led to the emergence of a new class of materials with novel properties and a very high specific surface area. Nanosheets of a wide range of materials have been synthesized including polyanionic cathodes like $LiFePO_4$, $LiMnPO_4$, and $LiCoPO_4$ which show improved high rate performance and cycle stability compared to bulk materials [41]. Rangappa et al. [42] applied the supercritical fluid technique to form

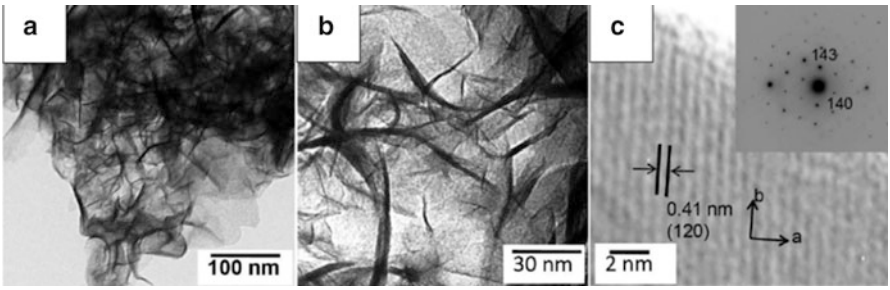

Fig. 2.11 TEM images of the as-prepared samples. (**a** and **b**) Li_2MnSiO_4 nanosheets; (**c**) HRTEM images of Li_2MnSiO_4 nanosheets with SAED patterns in the inset (Reprinted with permission from Rangappa et al. ([42]). Copyright (2012) American Chemical Society)

nanosheets of Li_2MnSiO_4 with a thickness of only several atoms and lateral dimensions of 100–300 nm (Fig. 2.11a–c). Nanosheet morphology has the advantage of dramatically reducing the lithium ion diffusion length in the material and also potentially accommodating the volumetric changes associated with lithium extraction and insertion. However, the complex synthetic pathway made it difficult to control the phase purity of the product, and x-ray analysis results revealed the presence of peaks of unidentified impurities. The electrochemical results showed high discharge capacities above 300 $mAhg^{-1}$ for the first 20 cycles at 45 °C and a current rate of 0.02 C, followed by a reported dramatic loss of capacity (Fig. 2.12). This loss of capacity was probably due to structural collapse of the Li_2MnSiO_4 as x-ray diffraction of cathodes after cycling showed no remaining peaks of the initial Li_2MnSiO_4 phase. This indicates that the nanosheet morphology was not successful in overcoming the structural instability associated with lithium insertion and extraction in Li_2MnSiO_4. However, the nanosheet morphology was successful in reducing the polarization of the cathodes resulting in a gently sloping discharge curve and high capacities. Unfortunately no cycling data was given for higher current rates as it is in this regime that the benefits of this morphology are likely to be most significant.

2.5.7.3 The Use of Surfactants to Create Complex Nanostructures

Deveraju et al. [43] performed synthesis reactions using the supercritical fluid technique and incorporating surfactants in the synthesis. By varying the amount and nature of the surfactant, the reaction time, and temperature, they formed samples with a wide range of particle sizes and morphologies, including monodisperse nanoparticles and complex, hierarchical structures (Fig. 2.13). Carbon coating was achieved by wet milling with PEDOT and carbon black followed by heat treatment at 450 °C in a reducing atmosphere. The complex synthesis resulted in somewhat impure products in which it was difficult to control the phase content. No detailed structural analysis was performed on the products. The electrochemical

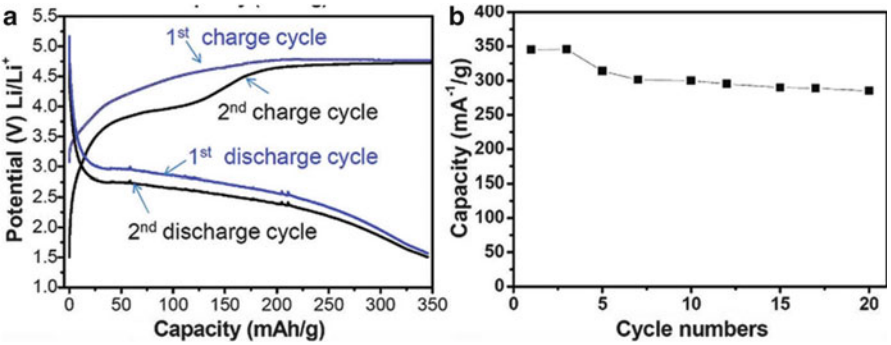

Fig. 2.12 Charge and discharge profile of first and second cycles. (**a**) Li_2MnSiO_4 samples measured at 45 °C temperatures at 0.02 C rates. (**b**) The cyclic performance of Li_2MnSiO_4 samples (Reprinted with permission from Rangappa et al. [42]. Copyright (2012) American Chemical Society)

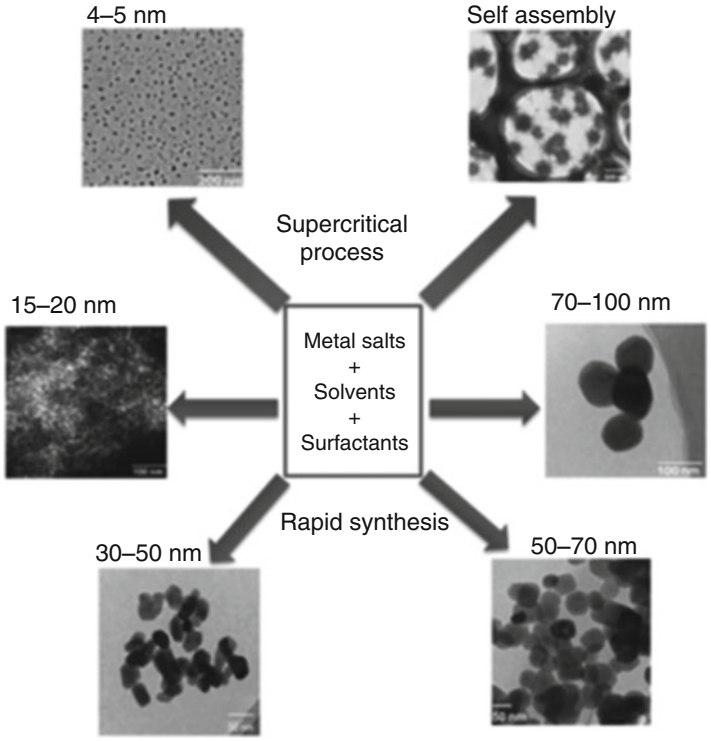

Fig. 2.13 Schematic of nanocrystalline Li_2MnSiO_4 positive electrode materials obtained via a supercritical fluid process and rapid reaction times (4–30 min). The process enables the synthesis of particles with a diameter of between 4 and 100 nm (Reprinted from Devaraju et al. [43] with permission of the Royal Society of Chemistry)

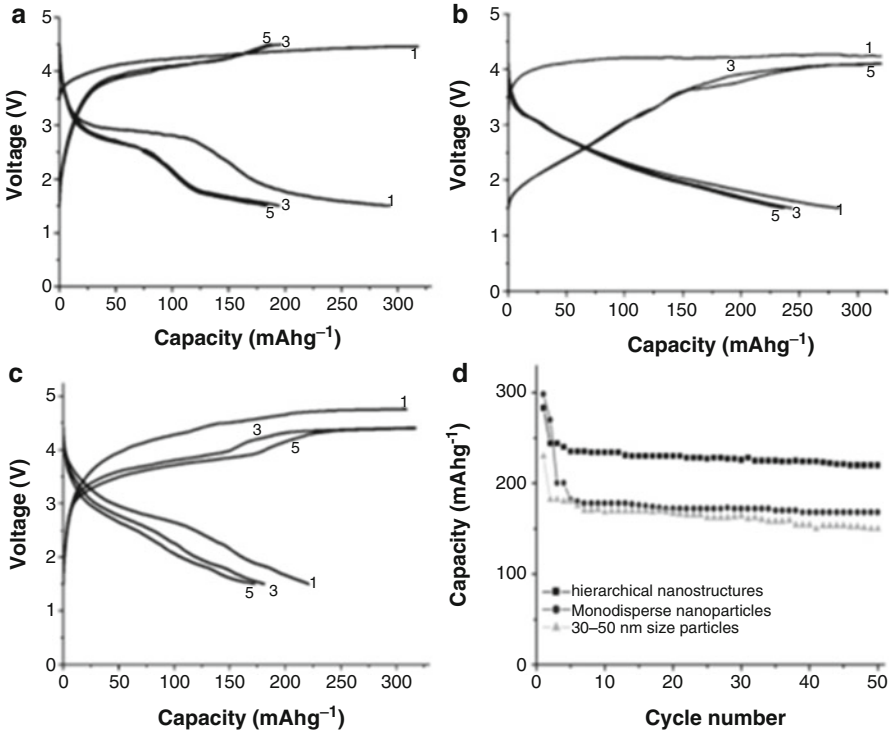

Fig. 2.14 Charge–discharge characteristics of Li_2MnSiO_4-positive electrode materials and cycle performance measured at room temperature with 0.05 C. (**a**) Charge–discharge curves of monodisperse nanoparticles showing typical two-step discharge profiles; (**b**) charge–discharge curves of hierarchical nanostructures showing a gentle slope-like discharge profile and nearly two lithium ion capacity for the first cycle and more than one lithium capacity for the 3rd and 5th cycles; (**c**) charge–discharge curves of 30–50 nm sized particles, with more than one lithium capacity for the 1st and 3rd cycles and nearly one lithium ion capacity for the 5th cycle; and (**d**) the cycle performance. The hierarchical nanostructures showed excellent cycling performance with a stable capacity up to 50 cycles; monodisperse particles showed a decrease in cycle performance after a few cycles due to detachment from the carbon source; 30–50 nm sized particles showed decent cycle performance (Reprinted from Devaraju et al. [43] with permission of the Royal Society of Chemistry)

performance of several of these materials is shown in Fig. 2.14. The highest capacities were reported for the complex hierarchical structures (Fig. 2.14b) although the average voltage was lower than that of the nanoparticle electrodes due to the absence of the voltage plateau region (Fig. 2.14a). Excellent capacity retention with cycling was observed but it should be noted that the composite cathodes contained about 40 w% carbon. This high carbon content would reduce the energy density of the cathodes. Good cycling stability with high carbon loading was earlier reported by Aravindan et al. [44].

2.5.8 Using Carbon Supports

2.5.8.1 Reduced Graphene Oxide Networks

Reduced graphene oxide (RGO) has recently attracted interest as a cathode material for lithium-ion batteries, and it has been demonstrated that Faradaic reactions occur between lithium and functional groups on the graphene oxide surface [45]. Zhao et al. [46] reported the use of carbon coating and a reduced graphene oxide network to support homogenously distributed nanoparticles of Li_2MnSiO_4 (Fig. 2.15). The x-ray diffraction data indicate the presence of the $Pmn2_1$ polymorph of Li_2MnSiO_4 with a minor MnO impurity. The electrochemical capacity at low current rates (0.05 C) was reported to be 290 $mAhg^{-1}$, and, even at the 1C rate, the material delivered a capacity of 170 $mAhg^{-1}$ after 700 cycles based on the mass of the Li_2MnSiO_4 (Fig. 2.16a and b). The total carbon content in the composite was calculated to be 26 % after synthesis, and a further 20 % of Ketjenblack was added to form the cathodes for electrochemical testing. At least some of the

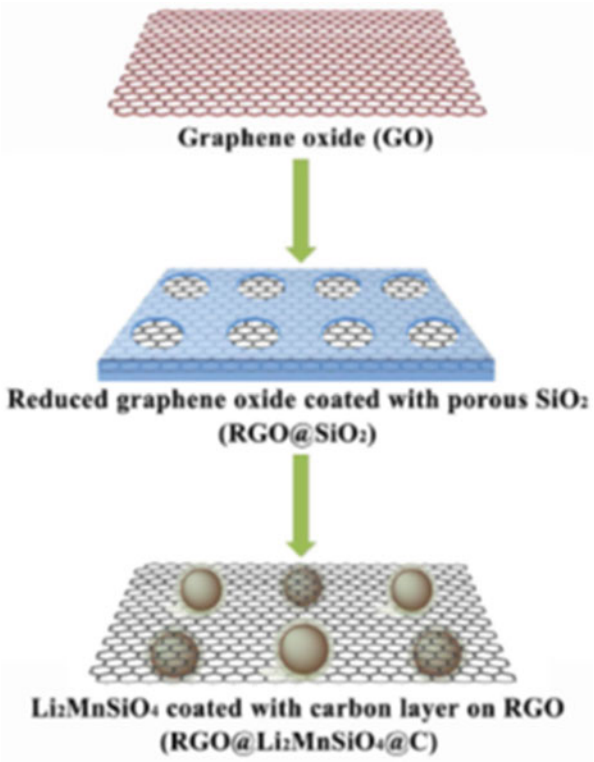

Fig. 2.15 Schematic synthesis of the RGO@Li_2MnSiO_4@C composite (Reprinted from Zhao et al. [46] with permission of the Royal Society of Chemistry)

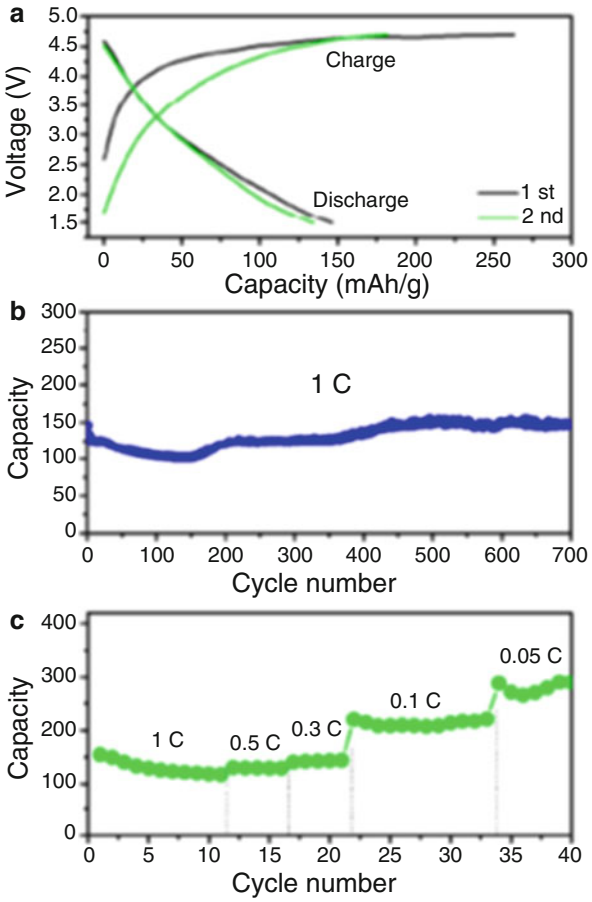

Fig. 2.16 (**a**) The first and second charge–discharge curves of the RGO@Li2MnSiO4@C composite at a current density of 1C between 1.5 and 4.7 V. (**b**) Discharge capacities vs. cycle number of the RGO@Li_2MnSiO_4@C composite at 1C. (**c**) Rate 5 performance of the RGO@Li_2MnSiO_4@C composite under various current densities (1C = 166 mA g-1) (Reprinted from Zhao et al. [46] with permission of the Royal Society of Chemistry)

observed capacity is likely due to the electrochemical activity of the RGO network itself, which is not taken into consideration in the capacity calculations [45]. The composite cathode had increased conductivity due to the presence of the conductive RGO, and the authors claimed that the RGO network and carbon coating prevented Mn dissolution into the electrolyte resulting in a stable electrochemical performance over 700 cycles in contrast to the findings of Rangappa et al. [42] who reported a dramatic capacity loss after 20 cycles. The high carbon loading is again a common factor in the cathodes that show good cycle stability over a large number of cycles, but would seriously reduce the energy density of the cathodes in practice.

2.5.8.2 Electrospinning to Form Li_2MnSiO_4/Carbon Nanofiber Cathodes

Electrospinning is a well-known technique that has been applied to produce fibers of many materials including silicon electrodes consisting of silicon nanoparticles encapsulated in a carbon sheath [47]. Earlier attempts to produce Cr-doped Li_2MnSiO_4 nanofibers resulted in material with a large MnO impurity [48]. The combined effect of Cr doping and nanofiber morphology showed an improved capacity and capacity retention with cycling compared to Li_2MnSiO_4 nanoparticles but the capacity faded with repeated cycling. Park et al. [49] used electrospinning to produce composite Li_2MnSiO_4/C nanofibers that consisted of nanoparticles of single-phase Li_2MnSiO_4 embedded in a carbon matrix (Fig. 2.17). The nanocrystals of the active phase and the carbon layer were synthesized simultaneously to

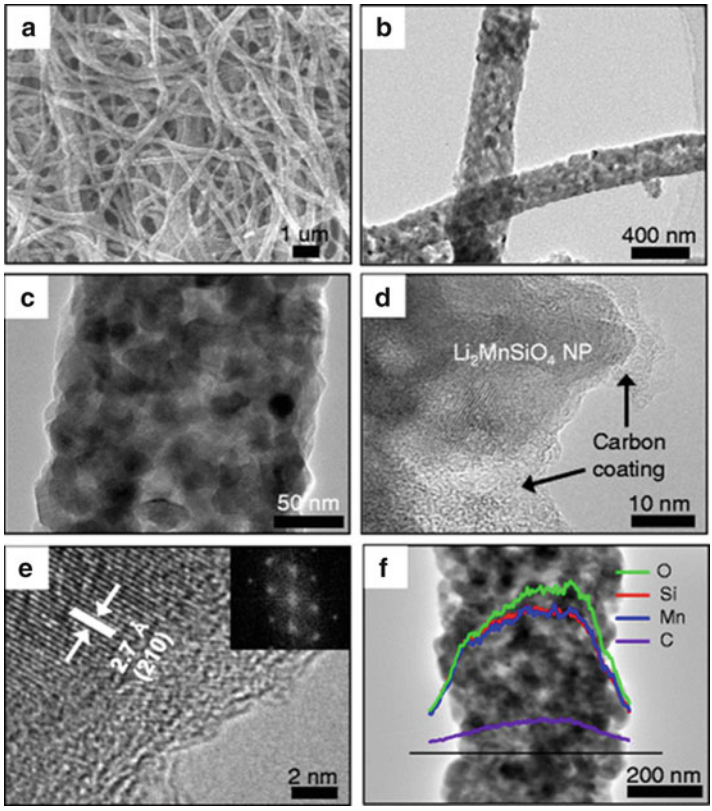

Fig. 2.17 (**a**) SEM image of as-spun Li_2MnSiO_4/C nanofibers, (**b**) low-magnification TEM image, (**c**) STEM image, (**d**) high-magnification TEM image, (**e**) HRTEM image, and (**f**) EDX line scan elemental mapping image for Li_2MnSiO_4/C nanofibers. The insert in e is the SAED pattern of Li_2MnSiO_4 (Reprinted from Park et al. [49], Fig. 2.1, copyright (2014). With kind permission from Springer Science and Business Media)

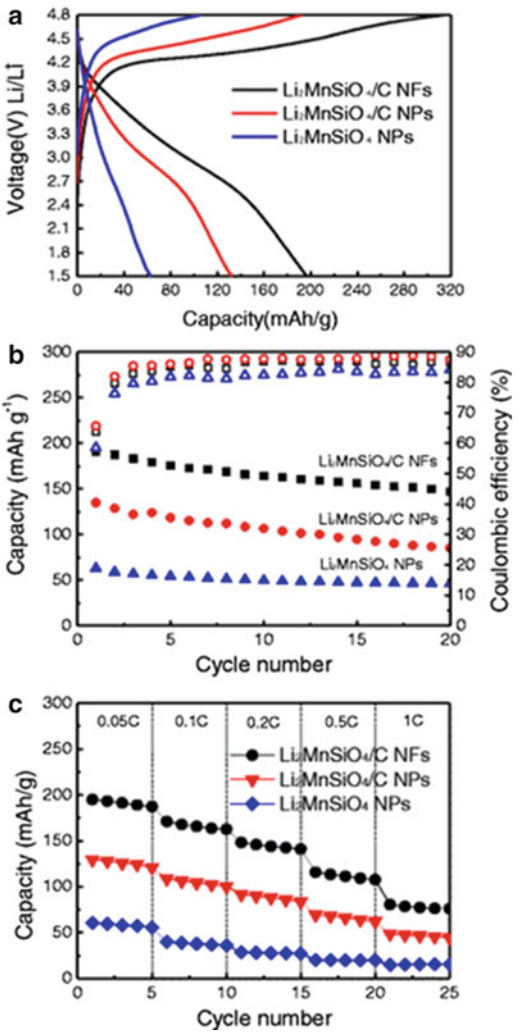

Fig. 2.18 The electrchemical properties of Li_2MnSiO_4 NPs, Li_2MnSiO_4/C NPs, and Li_2MnSiO_4/C NFs in the potential window of 1.5 ~ 4.8 V at a rate of 0.05 C at room temperature. (**a**) The first charge–discharge profile, (**b**) cycle performance, and (**c**) rate capability at various C rates (Reprinted from Park et al. [49], Fig. 2.1, copyright (2014). With kind permission from Springer Science and Business Media)

produce the composite product. The one-dimensional nanofibers had a diameter of approximately 400 nm, and Li_2MnSiO_4 nanoparticles of ~30 nm diameter were confined within the fibers. TGA analysis revealed that there was only ~6 wt% carbon in the nanofibers. The electrochemical performance of these composite nanofibers was shown to be superior to that of nanoparticles of Li_2MnSiO_4 as well as conventional carbon-coated nanoparticles with a first cycle discharge capacity of 197 mAg^{-1} at room temperature at a current rate of 0.05C (1C = 330 mAg^{-1}) (Fig. 2.18a). Capacity retention over 20 cycles was reported to be 77 %, comparable to that of the nanoparticulate samples tested, indicating that the amorphization commonly reported for these materials was not inhibited by the

nanofiber morphology (Fig. 2.18b). The one-dimensional nanofiber morphology was shown by impedance spectroscopy to improve the electron transport and rate capability of the Li_2MnSiO_4 nanofiber electrodes compared to electrodes consisting of active material with conventional carbon coating (Fig. 2.18c). However, the electrochemical capacity and capacity retention with cycling of the Li_2MnSiO_4 nanofiber electrodes was inferior to that reported for the RGO-supported material discussed in 5.8.1 although this may be as a consequence of the lower total carbon content in the electrode (~26 %) compared to ~46 % for the RGO composites [46].

2.5.9 Macroporous and Mesoporous Structures

Ordered porous materials with both macro- and mesopores have been synthesized and applied widely in materials chemistry. The use of ordered porous morphology for the active material in lithium ion battery electrodes has attracted much attention from researchers [50–55]. This method of nanostructuring cathodes has recently also been applied to polyanionic cathodes like $LiFePO_4$ [55, 56]. Porous cathodes have several advantages including the easy penetration of the electrolyte into the bulk of the material, the reduction of the diffusion distance in the thin walls of the pores, and the accommodation of volumetric changes in the material during lithium insertion and extraction [51]. Introducing porosity into cathodes unavoidably decreases the volumetric energy density of the material but, if the gain in performance is significant, then the actual practical energy density may still be improved [52].

2.5.9.1 Mesoporous, Carbon-Supported Li_2MnSiO_4

Kawase et al. [57] attempted to deposit Li_2MnSiO_4 nanoparticles within the mesopores of an ordered mesoporous carbon matrix as an alternative to a distributed carbon coating on the surface of nanoparticles. The carbon matrix would then function to enhance the conductivity of the composite cathode. However, x-ray diffraction analysis showed that these samples contained major impurities of MnO and that the peaks assigned to Li_2MnSiO_4 were poorly defined.

2.5.9.2 Mesoporous Cathodes from a Mesoporous Silica Template

Gummow and He [58] used a SBA-15 silica template and an emulsion synthesis technique to produce a Mn-deficient lithium manganese silicate product that retained the mesoporous symmetry of the SBA-15 precursor (Fig. 2.19). Cycling results for this material showed higher capacities and better capacity retention with cycling compared to nonporous material with the same composition (Fig. 2.20). This report showed the retention of the mesoporous symmetry with cycling although the crystallinity of the lithium manganese silicate was lost during the

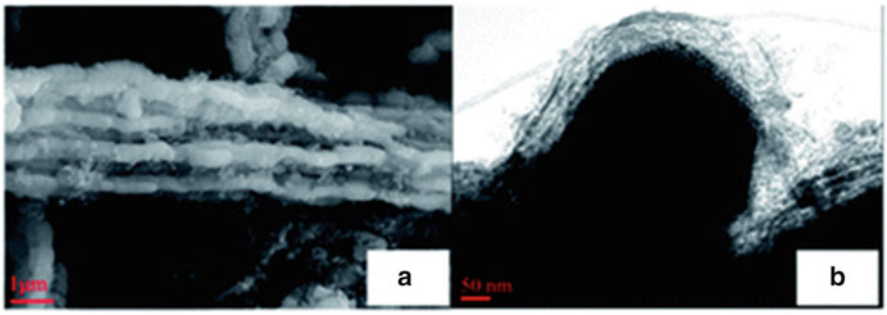

Fig. 2.19 Images of the mesoporous Mn-deficient lithium manganese silicate prepared from an SBA-15 mesoporous SiO_2 template (**a**) SEM image and (**b**) TEM image (Reproduced from Gummow and He [58] with permission of The Royal Society of Chemistry)

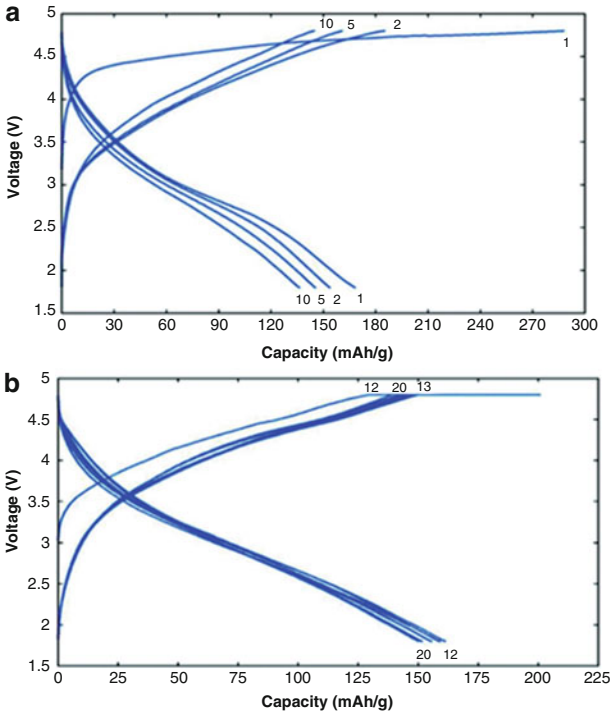

Fig. 2.20 Galvanostatic cycling curves of half cells containing mesoporous cathodes: (**a**) cycles 1–10 CC cycling and (**b**) cycles 12–20 CC–CV cycling at room temperature and 20 mAg^{-1} (Reproduced from Gummow and He [58] with permission of The Royal Society of Chemistry)

cycling process. This indicated that the amorphization previously reported for this material was not prevented by the mesoporous morphology. However, despite this loss of crystallinity, the sample cycled with excellent reversibility in the constant current-constant voltage regime.

2.5.9.3 Hierarchical Macroporous and Microporous Li_2MnSiO_4

He and Manthiram [59] reported the use of hierarchical macro- and mesoporous Li_2MnSiO_4 cathodes produced using a hard template of close-packed 430 nm diameter poly(methyl methacrylate) (PMMA) spheres. The PMMA template was impregnated with the precursors for Li_2MnSiO_4 as well as a resin as carbon source. After decomposing the PMMA by heating in an inert atmosphere, a replicated, ordered macroporous Li_2MnSiO_4 product was formed with average pores of 200–400 nm (Fig. 2.21a–c). The pore walls were composed of 20–40 nm nanocrystals of Li_2MnSiO_4 with additional disordered mesopores between the nanocrystals in the walls. Decomposition of the resin also provided a carbon coating on the surface of the nanocrystals to improve electrical conductivity with ~20 wt.% residual carbon in the composite cathodes. In electrochemical testing, the maximum discharge capacity reached was 200 $mAhg^{-1}$ on the 3rd discharge cycled at C/10 (16 mAg^{-1}) at 45 °C. At higher current rates, C/2 and C, the highest recorded capacities were 160 and 119 $mAhg^{-1}$, respectively. Capacity retention was good with about 112 % of the initial capacity reported after 40 cycles at 1 C (95 $mAhg^{-1}$) with a total carbon content in electrodes of ~30 %. Higher capacities

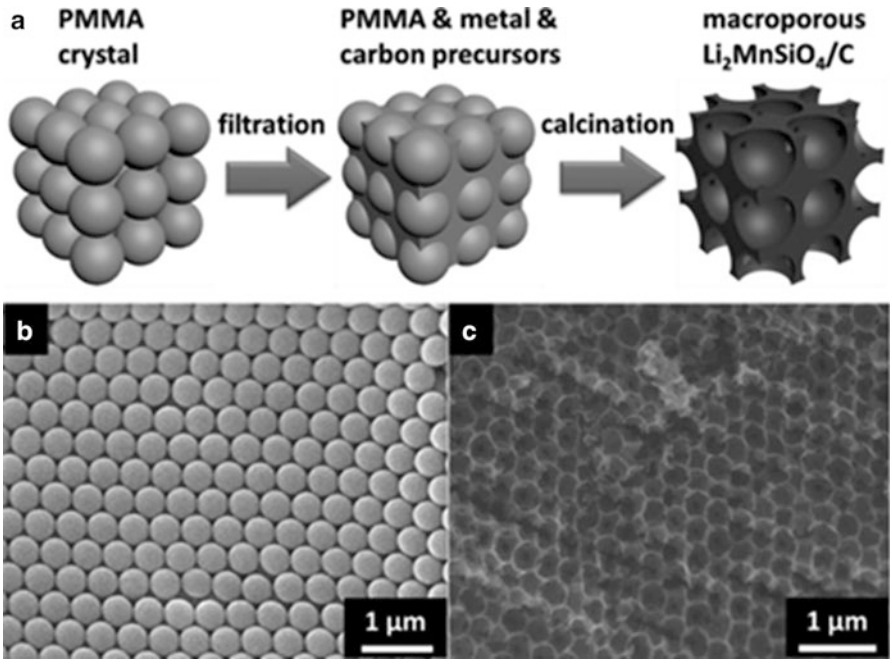

Fig. 2.21 (**a**) Schematic representation of the preparation process of the hierarchical ordered macroporous Li_2MnSiO_4/C with PMMA as the hard template; SEM images of the (**b**) PMMA spheres and (**c**) the resulting Li_2MnSiO_4/C replica (Reprinted from He and Manthiram [59]. Copyright (2014) WILEY-VCH Verlag GmbH & Co. KGaA, Weinheim with permission)

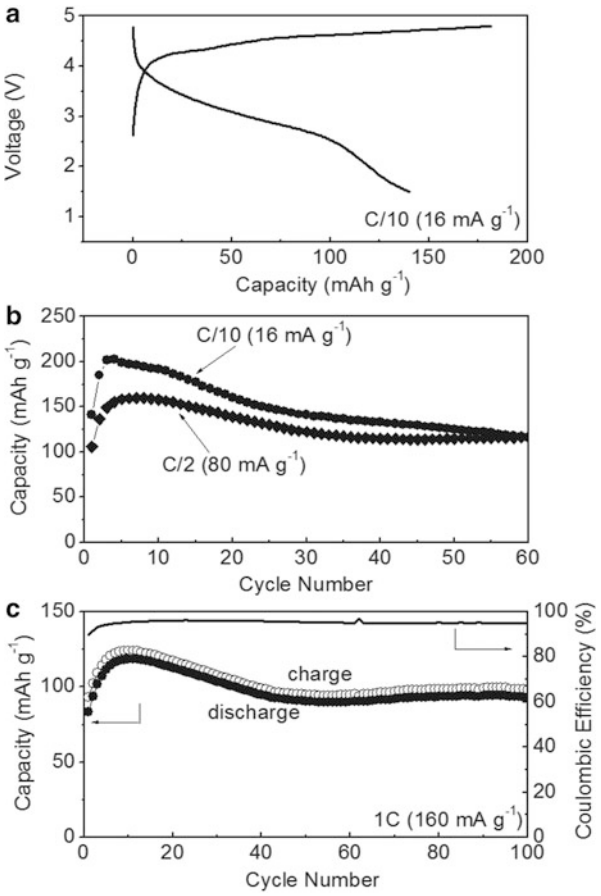

Fig. 2.22 Electrochemical performance of the Li 2 MnSiO 4/C cathodes at 45 °C: (**a**) initial charge–discharge profile at C/10, (**b**) cycling performance at C/10 and C/2, (**c**) cycling performance and Coulombic efficiency over 100 cycles at 1 C rate (Reprinted from He and Manthiram [59]. Copyright 2014 WILEY-VCH Verlag GmbH & Co. KGaA, Weinheim with permission)

were recorded for cells cycled at 55 °C but the capacity retention with cycling was reduced and found to be very sensitive to the voltage range that was chosen (Fig. 2.22).

2.6 Spray Pyrolysis

Spray pyrolysis is a commonly used technique to produce ceramic powders with a well-defined composition and a narrow particle size distribution [60]. Spray pyrolysis, combined with high-energy ball milling, has recently been applied to form Li_2MnSiO_4/C composites using glucose as the carbon source [61–63]. Shao and Taniguchi found the best performance for composites produced with a 0.1 mol l^{-1} glucose solution to give 12 wt% residual carbon in the composite and 15.2 wt% C in

the electrodes with primarily particles in the 40 nm range. The 1st cycle discharge capacity was approximately 170 $mAhg^{-1}$ at a current rate of 0.1 C with cycling in the range 1.5–4.8 V. However, even with this optimized composition, the cathodes showed poor capacity retention with cycling at room temperature with a residual capacity of only ~100 mAg^{-1} after 20 cycles. Moriya et al. [61] adopted a very similar strategy except that in their synthesis the glucose was added into the mixture prior to the pyrolysis step. In this way, the glucose was carbonized at the same time as the formation of the Li_2MnSiO_4 powder. The residual carbon in the composite was also determined to be 12 wt% in close agreement to the study of Shao et al. [63] but the composite electrodes consisted of 20 mg of active material and 15 mg of teflonized acetylene black (TAB) resulting in a much higher carbon loading in the electrodes than in the case of Shao et al. The particle size was also found to be only 10–20 nm and particles had an amorphous carbon coating. Moriya et al. [61] reported a stable discharge capacity of ~200 $mAhg^{-1}$ at 0.1 C and 25 °C for 60 cycles but it should be noted that the lower voltage cutoff was 1 V and the capacity above 1.5 V was only approximately 150 $mAhg^{-1}$. The authors also found it necessary to replace the anode and anode current collector after every 20 cycles because of degradation during cycling. This further serves to confirm the findings of other investigators [44, 46] that stable cycling of Li_2MnSiO_4 cathodes is possible with high carbon loading. Moriya et al. [62] carried out a detailed structural analysis of cycled cathodes of their spray-pyrolyzed Li_2MnSiO_4 material. The material could be indexed as the $Pmn2_1$ orthorhombic polymorph of Li_2MnSiO_4. In contrast to other structural studies, Moriya et al. found that although the long-range order of the sample was lost on charge, when lithium was subsequently reinserted on discharge, the peaks corresponding to Li_2MnSiO_4 re-appeared (Fig. 2.23). Pair distribution function (PDF) analysis indicated that the local structural order was disrupted when lithium was extracted due to local distortions of the MnO tetrahedra to accommodate the smaller Mn^{3+} and Mn^{4+} cations generated on charge. Importantly, the structural order was restored when lithium was reinserted, as evidenced by the re-appearance of the diffraction peaks.

2.7 Conclusion

After more than 15 years of research effort by lithium-ion battery researchers, there is now a good understanding of many of the structural and electrochemical properties of Li_2MnSiO_4. The wide range of synthesis methods and nanostructuring strategies that have been explored shows the persistence and determination of researchers to find the optimum methods to get the most out of this material in terms of electrochemical performance. Sophisticated nanostructures, e.g., nanosheets, nanofibers, and complex hierarchical porous structures, have been formed and have delivered dramatic improvements in high rate performance due to the increased surface area for interaction with the electrolyte and the reduced diffusion length for lithium ions. Recent structural studies by Moriya et al. [62]

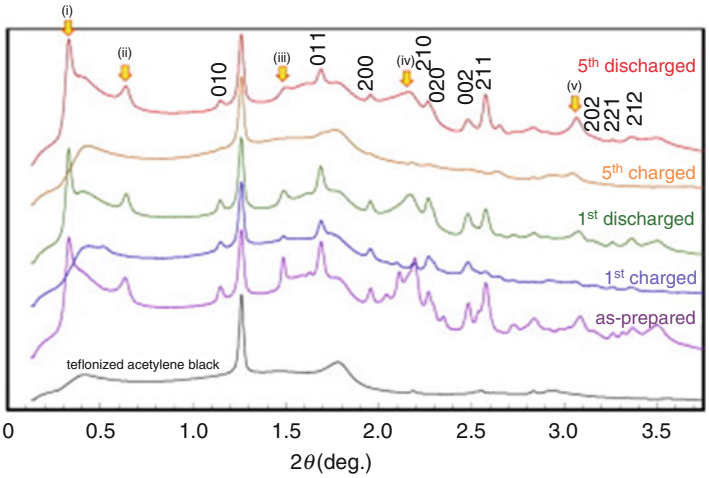

Fig. 2.23 Synchrotron-based HE-XRD patterns of the as-prepared, 1st-charged, 1st-discharged, 5th-charged, and 5th-discharged samples and the teflonized acetylene black. The carbon-hybridized Li_2MnSiO_4 samples were charged or discharged in the delithiation of 1.25 Li/formula unit. The hkl indices refer to the underlining β-Li_2MnSiO_4 structure (Reprinted from Moriya et al. [62]. Copyright 2014, with permission from Elsevier)

have also indicated that nanostructuring, coupled with high carbon loading, can allow the structure to reversibly accommodate the distortions to the MnO_4 tetrahedra that inevitably occur with Li extraction.

References

1. Nagaura T, Tozawa K (1990) Prog Batter Solar Cells 9:209
2. Armand M, Tarascon JM (2008) Building better batteries. Nature 451:652–657
3. Thackeray MM, Wolverton C, Isaacs ED (2012) Electrical energy storage for transportation-approaching the limits of, and going beyond, lithium-ion batteries. Energy Environ Sci 5:7854–7863
4. Xu T, Wang W, Gordin ML et al (2010) Lithium-ion batteries for stationary energy storage. JOM-US 62:24–30
5. Arico AS, Bruce P, Scrosati B et al (2005) Nanostructured materials for advanced energy conversion and storage devices. Nat Mater 4:366–377
6. Song T, Xia J, Lee J-H et al (2010) Arrays of sealed silicon nanotubes as anodes for lithium ion batteries. Nano Lett 10:1710–1716
7. Wang Y, Zeng HC, Lee JY (2006) Highly reversible lithium storage in porous SnO_2 nanotubes with coaxially grown carbon nanotube overlayers. Adv Mater 18:645–649
8. Armand M (2002) World Patent WO02/27823
9. Padhi AK, Nanjundaswamy KS, Goodenough JB (1997) Phospho-olivines as positive-electrode materials for rechargeable lithium batteries. J Electrochem Soc 144:1188–1194
10. Nazar LF, Goward G, Leroux F et al (2001) Nanostructured materials for energy storage. Int J Inorg Mater 3:191–200

11. Ravet N, Chouinard Y, Magnan JF et al (2001) Electroactivity of natural and synthetic triphylite. J Power Sources 97–98:503–507
12. Ellis BL, Lee KT, Nazar LF (2010) Positive electrode materials for Li-ion and Li-batteries. Chem Mater 22:691–714
13. Gong Z, Yang Y (2011) Recent advances in the research of polyanion-type cathode materials for Li-ion batteries. Energy Environ Sci 4:3223–3242
14. Islam MS, Dominko R, Masquelier C et al (2011) Silicate cathodes for lithium batteries: alternatives to phosphates? J Mater Chem 21:9811–9818
15. Dominko R, Bele M, Gaberscek M et al (2006) Structure and electrochemical performance of Li_2MnSiO_4 and Li_2FeSiO_4 as potential Li-battery cathode materials. Electrochem Commun 8:217–222
16. Dominko R, Bele M, Kokalj A et al (2007) Li_2MnSiO_4 as a potential Li-battery cathode material. J Power Sources 174:457–461
17. Lv D, Bai J, Zhang P et al (2013) Understanding the high capacity of $Li_2FeSiO4$: in situ XRD/XANES study combined with first principles calculations. Chem Mater 25:2014–2020
18. Dominko R, Sirisopanaporn C, Masquelier C et al (2010) On the origin of the electrochemical capacity of Li $_2Fe_{0.8}Mn_{0.2}SiO_4$. J Electrochem Soc 157:A1309
19. Bruce PG, Lyness C, Delobel B et al (2007) The lithium intercalation compound Li_2CoSiO_4 and its behaviour as a positive electrode for lithium batteries. Chem Commun 46:4890–4892
20. Gong ZL, Li YX, Yang Y (2007) Synthesis and electrochemical performance of Li_2CoSiO_4 as cathode material for lithium ion batteries. J Power Sources 174:524–527
21. Gummow RJ, Sharma N, Peterson VK et al (2012) Crystal chemistry of the Pmnb polymorph of $Li_2MnSiO4$. J Solid State Chem 188C:32–37
22. Politaev VV, Petrenko AA, Nalbandyan VB et al (2007) Crystal structure, phase relations and electrochemical properties of monoclinic Li_2MnSiO_4. J Solid State Chem 180:1045–1050
23. Duncan H, Kondamreddy A, Mercier PHJ et al (2011) Novel Pn polymorph for Li_2MnSiO_4 and its electrochemical activity as a cathode material in Li-ion batteries. Chem Mater 23:5446–5456
24. Gummow RJ, He Y (2014) Recent progress in the development of Li_2MnSiO_4 cathode materials. J Power Sources 253:315–331
25. Arroyo-deDompablo ME, Dominko R, Gallardo-Amores JM et al (2008) On the energetic stability and electrochemistry of Li_2MnSiO_4 polymorphs. Chem Mater 20:5574–5584
26. Gummow RJ, Sharma N, Peterson VK et al (2012) Synthesis, structure, and electrochemical performance of magnesium-substituted lithium manganese orthosilicate cathode materials for lithium-ion batteries. J Power Sources 197:231–237
27. Kuganathan N, Islam MS (2009) Li_2MnSiO_4 lithium battery material: atomic-scale study of defects, lithium mobility, and trivalent dopants. Chem Mater 21:5196–5202
28. Fisher CAJ, Kuganathan N, Islam MS (2013) Defect chemistry and lithium-ion migration in polymorphs of the cathode material Li_2MnSiO_4. J Mater Chem A 1:4207–4214
29. Dominko R (2008) Li_2MSiO_4 (M = Fe and/or Mn) cathode materials. J Power Sources 184:462–468
30. Kokalj A, Dominko R, Mali G et al (2007) Beyond one-electron reaction in Li cathode materials: designing $Li_2Mn_xFe_{1-x}SiO_4$. Chem Mater 19:3633–3640
31. Li YX, Gong ZL, Yang Y (2007) Synthesis and characterization of Li_2MnSiO_4/C nanocomposite cathode material for lithium ion batteries. J Power Sources 174:528–532
32. Wang Y, Li H, He P et al (2010) Nano active materials for lithium-ion batteries. Nanoscale 2:1294–1305
33. Deng C, Zhang S, Fu BL et al (2010) Characterization of $Li_2MnSiO4$ and Li_2FeSiO_4 cathode materials synthesized via a citric acid assisted sol–gel method. Mater Chem Phys 120:14–17
34. Belharouak I, Abouimrane A, Amine K (2009) Structural and electrochemical characterization of Li_2MnSiO_4 cathode material. J Phys Chem C 113:20733–20737
35. Liu WG, Xu YH, Yang R (2010) Synthesis and electrochemical properties of Li_2MnSiO_4/C nanoparticles via polyol process. Rare Met 29:511–514

36. Mali G, Meden A, Dominko R (2010) Li-6 MAS NMR spectroscopy and first-principles calculations as a combined tool for the investigation of Li_2MnSiO_4 polymorphs. Chem Commun 46:3306–3308
37. Manthiram A, Muraliganth T, Stroukoff KR (2010) Microwave-solvothermal synthesis of nanostructured Li_2MSiO_4/C (M = Mn and Fe) cathodes for lithium-ion batteries. Chem Mater 22:5754–5761
38. Kojima A, Kojima T, Tabuchi M et al (2012) Synthesis of Li_2MnSiO_4 cathode material using molten carbonate flux method with high capacity and initial efficiency. J Electrochem Soc 159: A532–A537
39. Kempaiah DM, Rangappa D, Honma I (2012) Controlled synthesis of nanocrystalline Li_2MnSiO_4 particles for high capacity cathode application in lithium-ion batteries. Chem Commun 48:2698–2700
40. Geim AK (2009) Graphene: status and prospects. Science 324:1530–1534
41. Rui X, Zhao X, Lu Z et al (2013) Olivine-Type nanosheets for lithium ion battery cathodes. ACS Nano 7:5637–5646
42. Rangappa D, Murukanahally KD, Tomai T et al (2012) Ultrathin nanosheets of Li_2MSiO_4 (M = Fe, Mn) as high-capacity Li-ion battery electrode. Nano Lett 12:1146–1151
43. Devaraju MK, Tomai T, Unemoto A et al (2013) Novel processing of lithium manganese silicate nanomaterials for Li-ion battery applications. RSC Adv 3:608–615
44. Aravindan V, Karthikeyan K, Kang KS et al (2011) Influence of carbon towards improved lithium storage properties of Li_2MnSiO_4 cathodes. J Mater Chem 21:2470–2475
45. Ha SH, Jeong YS, Lee YJ (2013) Free standing reduced graphene oxide film cathodes for lithium ion batteries. ACS Appl Mater Interfaces 5:12295–12303
46. Zhao Y, Wu C, Li J et al (2013) Long cycling life of Li_2MnSiO_4 lithium battery cathodes under the double protection from carbon coating and graphene network. J Mater Chem A 1:3856–3859
47. Hwang TH, Lee YM, Kong B-S et al (2011) Electrospun core–shell fibers for robust silicon nanoparticle-based lithium ion battery anodes. Nano Lett 12:802–807
48. Zhang S, Lin Z, Ji L et al (2012) Cr-doped Li_2MnSiO_4/carbon composite nanofibers as high-energy cathodes for Li-ion batteries. J Mater Chem 22:14661–14666
49. Park H, Song T, Tripathi R et al (2014) Li_2MnSiO_4/carbon nanofiber cathodes for Li-ion batteries. Ionics 20:1351–1359
50. Jiao F, Bruce PG (2007) Mesoporous crystalline β-MnO2—a reversible positive electrode for rechargeable lithium batteries. Adv Mater 19:657–660
51. Jiang C, Hosono E, Zhou H (2006) Nanomaterials for lithium ion batteries. Nano Today 1:28–33
52. Bruce PG (2008) Energy storage beyond the horizon: rechargeable lithium batteries. Solid State Ion 179:752–760
53. Jiao F, Bao J, Hill AH et al (2008) Synthesis of ordered mesoporous Li–Mn–O spinel as a positive electrode for rechargeable lithium batteries. Angew Chem Int Ed 47:9711–9716
54. Yan HW, Sokolov S, Lytle JC et al (2003) Colloidal-crystal-templated synthesis of ordered macroporous electrode materials for lithium secondary batteries. J Electrochem Soc 150: A1102–A1107
55. Doherty CM, Caruso RA, Smarsly BM et al (2009) Colloidal crystal templating to produce hierarchically porous $LiFePO_4$ electrode materials for high power lithium ion batteries. Chem Mater 21:2895–2903
56. Vu A, Stein A (2011) Multiconstituent synthesis of $LiFePO_4$/C composites with hierarchical porosity as cathode materials for lithium ion batteries. Chem Mater 23:3237–3245
57. Kawase T, Yoshitake H (2012) Cathodes comprising Li_2MnSiO_4 nanoparticles dispersed in the mesoporous carbon frameworks, CMK-3 and CMK-8. Microporous Mesoporous Mater 155:99–105
58. Gummow RJ, He Y (2014) Mesoporous manganese-deficient lithium manganese silicate cathodes for lithium-ion batteries. RSC Adv 4:11580–11584

59. He G, Manthiram A (2014) Nanostructured Li_2MnSiO_4/C cathodes with hierarchical macro-/mesoporosity for lithium-ion batteries. Adv Funct Mater 24:5277–5283
60. Messing GL, Zhang S-C, Jayanthi GV (1993) Ceramic powder synthesis by spray pyrolysis. J Am Ceram Soc 76:2707–2726
61. Moriya M, Miyahara M, Hokazono M et al (2014) Synthesis of hybrid Li_2MnSiO_4 nanoparticles with carbon for cathode materials with stable charge/discharge cycles. J Electrochem Soc 161:A97–A101
62. Moriya M, Miyahara M, Hokazono M et al (2014) High-energy X-ray powder diffraction and atomic-pair distribution-function studies of charged/discharged structures in carbon-hybridized Li_2MnSiO_4 nanoparticles as a cathode material for lithium ion batteries. J Power Sources 263:7–12
63. Shao B, Taniguchi I (2014) Synthesis of Li_2MnSiO_4/C nanocomposites for lithium battery cathode employing sucrose as carbon source. Electrochim Acta 128:156–162

http://www.springer.com/978-3-319-26080-8

Nanomaterials in Advanced Batteries and Supercapacitors

Ozoemena, K.I.; Chen, S. (Eds.)
2016, XV, 567 p. 261 illus., 189 illus. in color.,
Hardcover
ISBN: 978-3-319-26080-8